PNAS RESEARCH ARTICLE | IMMUNOLOGY AND INFLAMMATION

DIDO is necessary for the adipogenesis that promotes diet-induced obesity

María Ángeles García-López[a], Alfonso Mora[b], Patricia Corrales[c], Tirso Pons[a], Ainhoa Sánchez de Diego[a], Amaia Talavera Gutiérrez[a], Karel H. M. van Wely[a], Gema Medina-Gómez[c], Guadalupe Sabio[b], Carlos Martínez-A[a], and Thierry Fischer[a,1]

Edited by Tak Mak, University of Toronto, Toronto, Canada; received January 13, 2023; accepted October 24, 2023

The prevalence of overweight and obesity continues to rise in the population worldwide. Because it is an important predisposing factor for cancer, cardiovascular diseases, diabetes mellitus, and COVID-19, obesity reduces life expectancy. Adipose tissue (AT), the main fat storage organ with endocrine capacity, plays fundamental roles in systemic metabolism and obesity-related diseases. Dysfunctional AT can induce excess or reduced body fat (lipodystrophy). *Dido1* is a marker gene for stemness; gene-targeting experiments compromised several functions ranging from cell division to embryonic stem cell differentiation, both in vivo and in vitro. We report that mutant mice lacking the DIDO N terminus show a lean phenotype. This consists of reduced AT and hypolipidemia, even when mice are fed a high-nutrient diet. DIDO mutation caused hypothermia due to lipoatrophy of white adipose tissue (WAT) and dermal fat thinning. Deep sequencing of the epididymal white fat (Epi WAT) transcriptome supported *Dido1* control of the cellular lipid metabolic process. We found that, by controlling the expression of transcription factors such as C/EBPα or PPARγ, *Dido1* is necessary for adipocyte differentiation, and that restoring their expression reestablished adipogenesis capacity in *Dido1* mutants. Our model differs from other lipodystrophic mice and could constitute a new system for the development of therapeutic intervention in obesity.

adipose tissue | hypothermia | lipid metabolism | C/EBPα | PPARγ

Significance

Adipose tissue (AT), the main fat storage organ, has fundamental roles in systemic metabolism and in obesity-related diseases. Adiposity and lipodystrophy are associated with metabolic disorders, indicating that normal AT function is needed for metabolic health. Using mice bearing a DIDO mutant lacking the N terminus, we report that these animals show a lean phenotype with reduced adipose tissue and hypolipidemia, even when fed an obesogenic diet. The phenotype was linked with impaired adipogenesis that was partially corrected by transcription factors C/EBPα or PPARγ expression and hypothermia. Molecular analysis shows that *Dido1* orchestrates adipogenesis and offers a model different from lipodystrophies described in mice. This model pioneers a unique path to understanding obesity and to identifying mechanisms for obesity intervention.

In addition to sex and age, body fat variations rely on genetic background and environmental factors such as diet and exercise (1). The adipose tissue (AT) is an organ critical for whole-body energy and metabolic homeostasis (2). White adipose tissue (WAT) acts as a lipid storage reservoir for energy, whereas brown adipose tissue (BAT) participates in adaptive thermogenesis, induced by cold; both are dynamic and are physiologically and morphologically distinct (3, 4). An endocrine function has been recognized for AT, which regulates physiology by hormone and adipokine production (5). The global prevalence of obesity, characterized by excess body fat, has become a significant public health issue with a worrisome rise in the number of affected individuals (6). Dysfunctional AT can manifest in various conditions, including cachexia or wasting syndrome observed in cancer patients that leads to fat loss (7). Lipodystrophies involve abnormal fat accumulation in tissues, whereas lipoatrophies are characterized by fat loss (8). Regardless of etiology, these conditions frequently associate with insulin resistance, dyslipidemia, hypertension, hepatosteatosis, and higher risk for cardiovascular diseases (9). Because these metabolic conditions coexist in obesity and lipodystrophies, the study of lipoatrophic mouse models could offer a step toward better understanding AT function and the metabolic syndrome (10).

In vertebrates, *Dido1* is a gene that gives rise to three messengers. In mouse, after maturation, *Dido1* encodes three protein isoforms, DIDO1 (614 amino acids), DIDO2 (1183 aa), and DIDO3 (2256 aa), with distinct functions from cell division to embryonic stem cell differentiation (11–14). DIDO1 binds to the E3 ubiquitin ligase WW domain-containing protein 2 (WWP2); both proteins participate in downregulation of the stemness marker OCT4 and are essential for primitive endoderm formation in mouse embryonic stem cells (14). DIDO2 and DIDO3 share a transcription elongation factor S-II subunit M (TFSIIM) domain, and a Spen paralog and ortholog (SPOC) module (15). In addition to the RNA POL II binding domains, DIDO3 contains a long C-terminal region (CT) that binds to the splicing factor proline- and glutamine-rich (SFPQ) for RNA splicing regulation (16) and to the ATP-dependent RNA helicase A (DHX9) for additional transcriptional control (17). All DIDO proteins share a common N-terminal plant homeodomain (PHD) with a regulatory histone-binding region (13). PHD-containing proteins and PHD zinc fingers regulate gene expression and cancer development (18). In mice, gene targeting with the deletion of exon 3 and 4 of *Dido1* (NT) results in myelodysplasias due to truncation of the initial 422 amino acids (19).

Author contributions: G.M.-G., G.S., C.M.-A., and T.F. designed research; M.Á.G.-L., A.M., P.C., A.S.d.D., G.S., and T.F. performed research; A.T.G. and K.H.M.v.W. contributed new reagents/analytic tools; T.P., K.H.M.v.W., G.S., and C.M.-A. analyzed data; and T.F. wrote the paper.

The authors declare no competing interest.

This article is a PNAS Direct Submission.

[1]To whom correspondence may be addressed. Email: tfischer@cnb.csic.es.

This article contains supporting information online at https://www.pnas.org/lookup/suppl/doi:10.1073/pnas.2300096121/-/DCSupplemental.

Published January 9, 2024.

Here, we studied the metabolic function of DIDO using DIDO truncation (ΔNT) in mouse. We found that, when fed a high-fat diet (HFD), these ΔNT mice have reduced weight gain associated with an improved metabolic profile. On the HFD, ΔNT produced protection against white AT hypertrophy and expansion in several adipose depots including epididymal, subcutaneous, and dermal. Our data clearly show a role for the DIDO NT domain in regulating AT differentiation, development, resistance to HFD, and obesity through C/EBPα and PPARγ gene expression. Knowledge of structural data for the NT domain offers the potential to identify and design new therapeutic tools for intervention in obesity.

Results

***Dido1* Function Is Crucial for In Vivo AT development In Vivo.** Litter sizes of the C57BL/6 DIDO colony ranged from two to nine pups with a mean of 5.5 ± 0.267 (n = 198); the most frequent litter size was five (*SI Appendix*, Fig. S1*H*). Birth weights within 10 h postpartum were similar for mutant mice (ΔNT; n = 9, 1.29 g ± 0.06), wild-type mice (WT; n = 10, 1.41 g ± 0.09), and heterozygotic mice (n = 17, 1.44 g ± 0.02). Glycemia levels were monitored and corresponded to ΔNT n = 9, 74.33 mg/dL ± 5.45, WT n = 10, 57.44 mg/dL ± 3.61, and heterozygotes n = 17, 70.28 mg/dL ± 2.54. ΔNT mice show embryonic lethality, with a 5.2% survival rate. Progeny had the expected sex ratio, with total female and partial male sterility. A normal diet (ND) was fed to male offspring, and weight gained was recorded for 21 wk (W21). Starting from W16, ΔNT on a ND were significantly lighter compared to WT littermates (Fig. 1*A*). Overall macroscopic examination of the peritoneal cavity of 29-wk-old ΔNT mice (W29) confirmed reduced adiposity (*SI Appendix*, Fig. S1*A*), lean phenotype, and reduced gonadal fat pads (*SI Appendix*, Fig. S1*B*). WAT, including posterior subcutaneous (SC) and epididymal (Epi) WAT, have reduced mass; no significant reductions were measured for brown adipose tissue (BAT), the liver, gastrocnemius, or soleus muscle (*SI Appendix*, Fig. S1*C*). In another experimental condition, mouse cohorts were fed a control diet (CD) for 8 wk, followed by 13 wk of CD or HFD; ΔNT mice were significantly leaner starting W12. ΔNT mice were resistant to ND and HFD-induced weight gain. In Epi, SC, and dermal WAT (D WAT), HFD triggered adipocyte growth and hypertrophy (Fig. 1 *B*, *D*, and *F*). This did not occur in ΔNT mice (Fig. 1 *C*, *E*, and *G*). Computer image analysis of adipocyte size confirmed that WAT from CD or HFD-fed WT mice had more adipocytes in the very large-sized bins, >9,001 μm^2 in Epi WAT (*SI Appendix*, Fig. S1*D*). In SC WAT in large bins (>1,001 μm^2) only HFD drove adipocyte expansion (*SI Appendix*, Fig. S1*E*). In ΔNT mice, D WAT resisted HFD-induced dermal adipocyte expansion (*SI Appendix*, Fig. S1*F*). In addition, HFD triggered thinning of the dermis, not seen in ΔNT mice (*SI Appendix*, Fig. S1*G*). Adipocytes from ΔNT WAT were smaller because of limited lipid droplet extensions.

Serum lipid profiling in animals fed with CD or HFD showed that following HFD, triglycerides (TG), LDL, total cholesterol, and HDL were reduced in ΔNT compared to WT littermates (Fig. 1 *H–K*). Nonesterified fatty acid (NEFA) levels were unchanged (*SI Appendix*, Fig. S1*I*). Reduced lipid content in ΔNT mice led us to evaluate blood adipokines such as the satiety hormone leptin, secreted in proportion to fat mass (20), and resistin. On a ND, low leptin levels were observed in ΔNT serum compared to WT littermates (*SI Appendix*, Fig. S2*A*), with no changes in resistin levels (*SI Appendix*, Fig. S2*B*). Leptin was related to skeletal growth (21); femoral bone length measured using digital

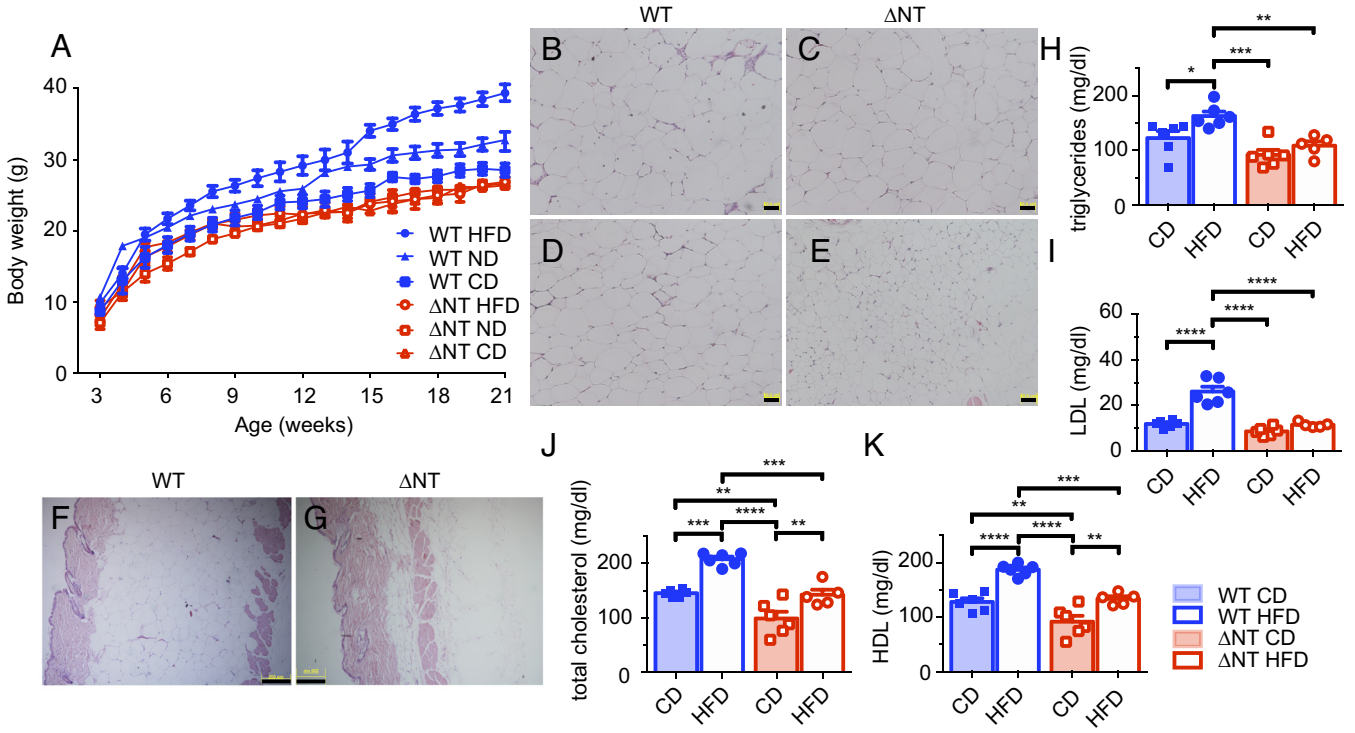

Fig. 1. Detained weight gains and hypolipidemia in mutant DIDO ΔNT mice fed a normal diet (ND), control diet (CD), or high fat diet (HFD). (*A*) Body weight gains in 3- to 21-wk-old mice. Data are mean ± SEM. WT HFD (n = 3–15, blue filled circles), WT ND (n = 4–12; blue filled triangles), WT CD (n = 3–10; blue filled squares): ΔNT HFD (n = 3–11; red open circles), ΔNT ND (n = 3–5; red open triangles) and ΔNT CD (n = 3–7; red open squares). (*B–K*) Mouse cohorts were placed on CD for 8 wk, followed by 13 wk of CD or HFD (*B–G*). HE staining of Epi WAT (*B* and *C*), SC WAT (*D* and *E*), and D WAT (*F* and *G*). [Scale bars, 50 μm (*B–E*) and 200 μm (*F* and *G*).] (*H*) Triglycerides, (*I*) LDL, (*J*) total cholesterol, and (*K*) HDL levels were registered in serum of mice fed with CD or HFD; individual and mean ± SEM. WT CD (n = 4, blue filled squares), WT HFD (n = 6; blue filled circles): ΔNT CD (n = 4; red open squares), and ΔNT HFD (n = 5; red open circles).

calipers showed that ΔNT mice suffered growth retardation (WT: 15.11 mm ± 0.18; ΔNT: 13.82 ± 0.18) (*SI Appendix*, Fig. S2*C*).

In summary, gene targeting of *Dido1* exons 3 and 4 (ΔNT) protects mice from ND- and HFD-induced weight gains. When on HFD, it affected Epi, SC, and D WAT development and expansion, and lowered circulating fat. ΔNT mice metabolized lipids well, despite their reduced adiposity. Unlike typical lipodystrophic conditions characterized by low leptin levels and ectopic fat accumulation in the liver or skeletal muscle (22), our findings demonstrated that the ΔNT mice had no inappropriate fat deposited in the liver (*SI Appendix*, Fig. S7 *C* and *D*) or skeletal muscle (*SI Appendix*, Fig. S5 *G* and *H*).

***Dido1* Targeting Results in Hypothermia.** Insulin and glucagon regulate glucose homeostasis. On ND, insulin levels were reduced in ΔNT mice (Fig. 2*A*). Lowered leptin levels in obesogenic conditions benefited body weight, glucose tolerance, and insulin sensitivity in mice (23). Glucose levels were monitored in animals on CD (*SI Appendix*, Fig. S3*A*) or HFD (*SI Appendix*, Fig. S3*B*), in fasted and fed states. Higher glycemic values were observed in the fed condition, with no differences between genotypes (*SI Appendix*, Fig. S3 *A* and *B*). Intraperitoneal (i.p.) glucose tolerance tests (GTT) on 2-h fasted CD (*SI Appendix*, Fig. S3*C*) and HFD mice (*SI Appendix*, Fig. S3*D*) showed little difference between genotypes.

During metabolic phenotyping of the mice, we observed notable differences in body temperatures (rectal) independent of the nutritional state, fasted or fed; ΔNT mice were hypothermic compared to WT littermates (Fig. 2*B*). Body temperature of ΔNT mice increased from the fasted to the fed state. In ΔNT mice, HFD equalized the hypothermia (Fig. 2*C*). The hypothermia might be explained by the reduction of the dermal fat layer in skin biopsies, as described above (Fig. 1 *F* and *G*). Reduced D WAT in skin leads to incomplete thermal insulation and a defective response to cold. Food intake (Fig. 3 *A* and *B*) and metabolic parameters monitored by indirect calorimetry in metabolic cages (Fig. 3 *C*–*F*) showed differences in the dark and light phase respiratory exchange ratio (RER) (Fig. 3 *C*–*E*) and energy expenditure (EE) (*SI Appendix*, Fig. S4 *A*–*C*). Changes in activities (*SI Appendix*, Fig. S4 *E* and *F*) and higher fecal lipid excretions, (*SI Appendix*, Fig. S2*D*) although not significant, could explain the leanness of the ΔNT mice. Based on the RER data, it appears that the ΔNT mice rely more heavily on carbohydrates than on lipids as an energy source. The significant changes in RER likely contribute to the leanness in ΔNT mice on a HFD compared to WT mice on the same diet. Small, even statistically non-significant changes in nocturnal activity, coupled with changes in RER and fecal lipids over several weeks, could result in body weight differences. Since insulin has a general anabolic function, low insulin levels could also contribute to low mass in ΔNT mice. Hypothermia can be attributed to abnormal dermal tissue development.

***Dido1* Regulates Lipases and Lipid Metabolism.** To examine the association between *Dido1* and AT maintenance and function, we conducted comparative analysis of the transcriptomes of WT and ΔNT Epi WAT from mice fed a CD or HFD. Deep sequencing and DESeq2 revealed significant changes in gene expression patterns. On the CD, we identified 47 genes that significantly changed (fold change > 1.5) with high confidence; of these, 9 are up- and 38 are down-regulated. Among the up-regulated genes in WT mice, we found *Bscl2* (*SI Appendix*, Fig. S10*C*), which is associated with lipodystrophy in humans and mice (9, 24). In our transcriptomics data, we also detected *Bcl6*, which is involved in the developmental expansion of SC versus Epi WAT (25). *Rbp4*, a vitamin A transporter and adipokine with a crucial function in metabolic syndrome (26), was also up-regulated.

On the HFD, a larger number of differentially expressed genes (DEG) was identified, with 377 up- and 348 down-regulated (Fig. 4*A* and Dataset S1). For functional enrichment analysis of the DEG, we used g:Profiler, which identified the most significant Gene Ontology (GO) molecular function (MF) terms including lipase activity (GO:MF 0016298), lipid kinase activity (GO:MF 0001737), and phospholipid and lipid binding (GO:MF 0005543) (Fig. 4*B* and Dataset S2). HFD or obesity drives immune cell infiltration, which explains the presence of an immune gene signature in WAT transcriptomes. HFD triggers fibrogenic functions and remodeling genes (ref. 27 and *SI Appendix*, Fig. S8 *A* and *B*). The heat map depicts the genes that encode lipases and phospholipases, including *Lipg*, *Pla2g16*, *Lipa*, *Pla1a*, *Pla2g7, and Pld3* (Fig. 4*C*), many of which form part of the 2-arachidonoylglycerol (2-AG) pathway (Lipidmaps.org). After functional classification by g:Profiler into "Biological Processes," additional DEG were identified in the GO and subcategorized (*SI Appendix*, Fig. S9). They represent the remainder of the heat map, with the detection of *Acsbg*1, *Alox12*, *Apoc*1, *Cyp2e1, Echdc2, Faah, Fads2, Mboat2, Mpzl2, Anxa1, Apobr, Cnr2, Daglb, Hacd4, Plin2, Soat1*, and *Ucp2*. The transcriptomics of Epi WAT on CD showed few variations in DEG, with no lipase or lipid metabolism gene changes (*SI Appendix*, Fig. S10 *A*–*C*).

***Dido1* Regulates Adipogenesis In Vitro.** The cell autonomous effect of *Dido1* was then evaluated in widely accepted models to study the function of genes in adipocyte differentiation and formation (28–30). Using SC WAT-derived mesenchymal

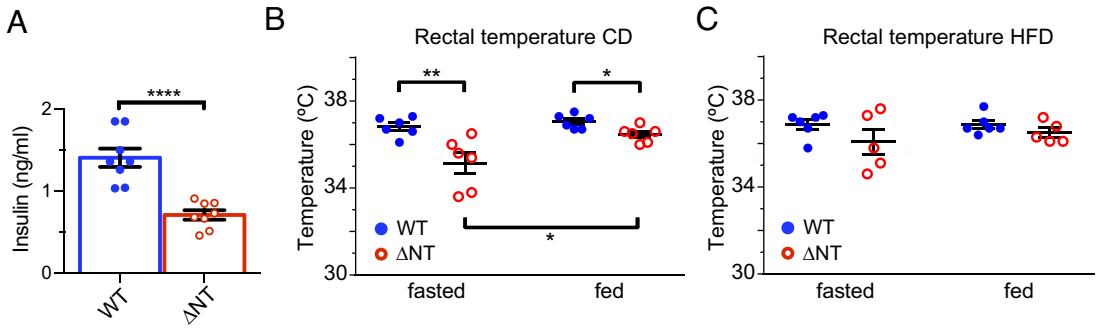

Fig. 2. Reduced insulin levels and body core temperatures in mutant ΔNT mice. (*A*) Insulin levels were measured after a 4-h fast in 27-wk-old mice fed a ND. WT: n = 8; ΔNT: n = 8. (*B*) Mice were fed a CD for 8 wk, followed by 13 wk of CD (*B*) or HFD (*C*), and body (rectal) temperatures were measured after a 6-h fast (fasted) or when refed (fed). WT (n = 6; blue filled circles): ΔNT (n = 5–6; red open circles). Data are individual and mean ± SEM.

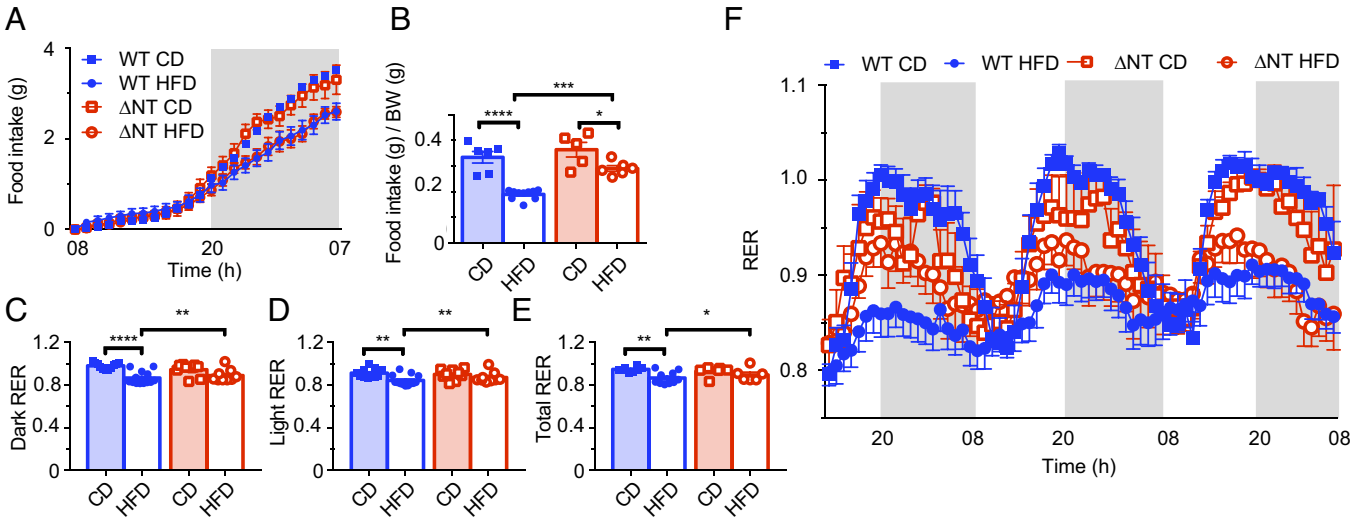

Fig. 3. ΔNT mice consumed more carbohydrates. Metabolic cage analysis of WT and ΔNT mice fed a CD or HFD to estimate night (dark), day (light), and total respiratory exchange ratio (RER). (*A*) Cumulative food intake is shown over a 24-h period. (*B*) Food intake was normalized with respective body weights. Mice eat more when on a CD. Analysis of the RER in (*C*–*F*). Night and day RER measured hourly over a 68-h period. WT on a CD consumed mainly carbohydrates as an energy source, whereas WT on a HFD metabolized a mix of lipids and carbohydrates. ΔNT CD and ΔNT HFD animals utilized a mix of carbohydrates and lipids. Significant changes were observed in the dark phase. Individual and mean ± SEM WT CD (n = 8–11, blue filled squares), WT HFD (n = 10–13; blue filled circles): ΔNT CD (n = 6–9; red open squares) and ΔNT HFD (n = 6–9; red open circles).

progenitors isolated after enzymatic digestion, we were able to differentiate the stromal vascular fraction (SVF) to adipocytes only in the presence of triiodothyronine (T3), insulin, dexamethasone (DEXA), indomethacin, 3-isobutyl-1-methylxanthine (IBMX), and rosiglitazone (30). After 7 to 9 d culture, refringent fat cells appeared only when derived from WT progenitors (Fig. 5 *A* and *B*), and lipids in cells were stained by oil red (ORO) (Fig. 5 *C* and *D*). In contrast, cells lacking *Dido1* were resistant to adipocyte differentiation.

In a second approach, we used multipotent mouse embryonic fibroblasts (MEF) from early mouse embryos. Following addition of an appropriate differentiation mix, MEF can differentiate into adipocytes or osteoblasts. MEF from WT or ΔNT embryos (dpc14.5) were differentiated to adipocytes (Fig. 5 *E* and *F*), after which ORO stained lipids efficiently in WT MEF (Fig. 5*E*), whereas ΔNT MEF remained unlabeled (Fig. 5*F*). When MEF were differentiated into osteoblasts, the osteoblast marker osteopontin labeled cell lysosomes equally well in both genotypes (Fig. 5 *G* and *H*). In ΔNT MEF, osteoblasteogenesis was possible, whereas adipogenesis was hindered.

We used western blot to track several adipogenesis markers in differentiated MEF lysates (Fig. 5*I*). Perilipin-1, PPARγ, adiponectin, and fatty acid binding protein 4 (FABP4) were lower in ΔNT MEF than in WT MEF cells. Perilipins are important regulators of lipid droplet formation and control obesity and insulin resistance (31). We determined relative mRNA levels of adipocyte-specific genes in MEF before (T0) and after differentiation (adipocytes, T10). RT-qPCR showed that levels of *Adipoq* (Fig. 5*J*), *Cebpa* (Fig. 5*K*), *Fabp4* (Fig. 5*L*), the glucose transporter type 4 *Glut4* (Fig. 5*M*), hormone-sensitive lipase *Lipe* (Fig. 5*N*), *Lpl* (Fig. 5*O*), phosphoenolpyruvate carboxykinase *Pepck* (Fig. 5*P*), perilipin-5 *Plin5* (Fig. 5*Q*), and *Pparγ* (Fig. 5*R*) were lower in ΔNT than in WT MEF after adipogenic differentiation. Adipogenesis is prevented in ΔNT MEF. Additional transcriptomics experiments with MEF after differentiation, and the same functional enrichment analysis (as in Fig. 4 *A*–*C*) showed that 1846 genes were up- and 1812 were down-regulated (*SI Appendix*, Fig. S11 *A* and *B*). This gene list included transcription factors mobilized during adipogenesis *Cebpa*, *Pparγ*, and *Srebf1*, lipases *Lipa, Pla2g4a, Pld3, Lipe, Lpl, Mgll, Pla2g16, PnPla2*, and lipid metabolism-regulating genes (*SI Appendix*, Fig. S11 *A* and *B*), which confirmed the importance of DIDO in adipogenesis in vivo and in vitro.

C/EBPα and PPARγ Restore Faulty Adipogenesis in NT Deletion of DIDO. Defective adipogenesis after DIDO truncation is subsequent to low expression of essential adipogenic genes, including *Cebpa* and *Pparγ*. PPARγ and C/EBPα are critical transcription factors for adipogenesis and work together to promote adipocyte differentiation. Several reports indicate that MEF with deficient adipogenesis due to lack of or reduction in PPARγ might recover adipogenesis potential by ectopic PPARγ expression (32, 33). To evaluate this possibility, we infected MEF with a retrovirus expressing green fluorescent protein (GFP) as control, with PPARγ2, C/EBPα, or a C/EBPα/PPARγ2 mixture. Differentiation evaluated by ORO staining (Fig. 6 *A*–*H*) was complete in WT MEF, regardless of the retroviral construct used (Fig. 6 *A*–*D*); in ΔNT MEF, no lipid staining was found with the GFP control (Fig. 6*E*). Overexpression of C/EBPα (Fig. 6*F*), PPARγ2 (Fig. 6*G*), or a mixture of both factors restored lipid droplet accumulation of smaller size (Fig. 6*H*). Adipocytic marker perilipin-1 distribution in differentiated MEF is shown by immunofluorescence (Fig. 6 *I*–*N*). No stain was detected in ΔNT MEF with control GFP (Fig. 6*L*). With ectopic expression of C/EBPα (Fig. 6*M*) or PPARγ2 (Fig. 6*N*), lipid droplets were restored after differentiation. Adipogenesis markers were investigated by western blot of MEF cell lysates after expressing GFP or PPARγ2 (Fig. 6*O*). Perilipin-1, PPARγ, and FABP4 were clearly rescued in ΔNT MEF. These findings suggest that *Dido1* acts upstream of *Pparγ* or *Cebpa* induction during adipogenesis.

Discussion

Dido1 mutations challenge the normal molecular steps of differentiation (13, 15). Here, we report the effects of a Dido1 mutation on metabolism in a mouse model, leading to a lean phenotype with low levels of circulating insulin and leptin and resistance to HFD. The ΔNT mice exhibit partial loss of endocrine function in their AT,

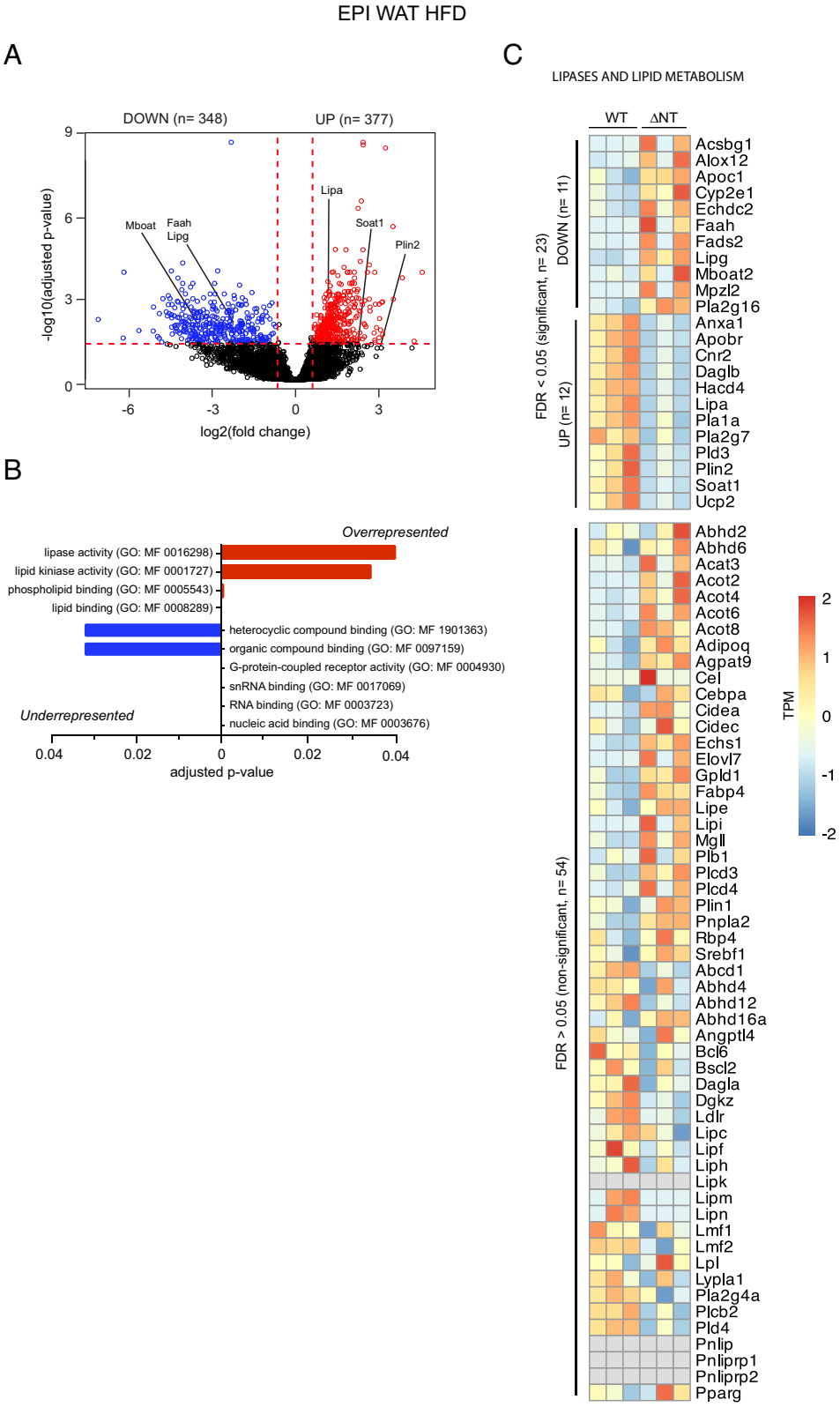

Fig. 4. Imbalanced gene expression of lipid metabolic process in Epi WAT of mice fed a HFD. Differentially expressed genes (DEG) were estimated after RNA-Seq analysis using DESeq2 in WT and ΔNT mice (CD 8 wk, followed by 13 wk of CD or HFD). (*A*) Volcano plot of the DEG for Epi WAT. *Lipa* and *Plin2* are up-regulated. (*B*) Significantly enriched GO terms for molecular functions (MF) after data analysis with g:Profiler statistical over- and underrepresentation test tool; $P < 0.05$. The term "lipases" is for GO molecular function terms: lipase activity, lipid kinase activity, phospholipid binding, and lipid binding. (*C*) Heat map showing normalized transcripts per million (TPM) of genes related to lipases and lipid metabolism (representing GO Biological Pathways terms linked to "lipids") across the WT and ΔNT transcripts.

leading to reduced leptin circulation. Our model is one of a genetically lean mouse with a reduced AT mass consisting of smaller adipocytes with reduced lipid content. The ΔNT mice suffer growth retardation and impaired TG storage in various AT, including Epi, SC and D WAT. The thinning of D WAT compromises the thermal insulation function, which explains the hypothermia observed in our mouse

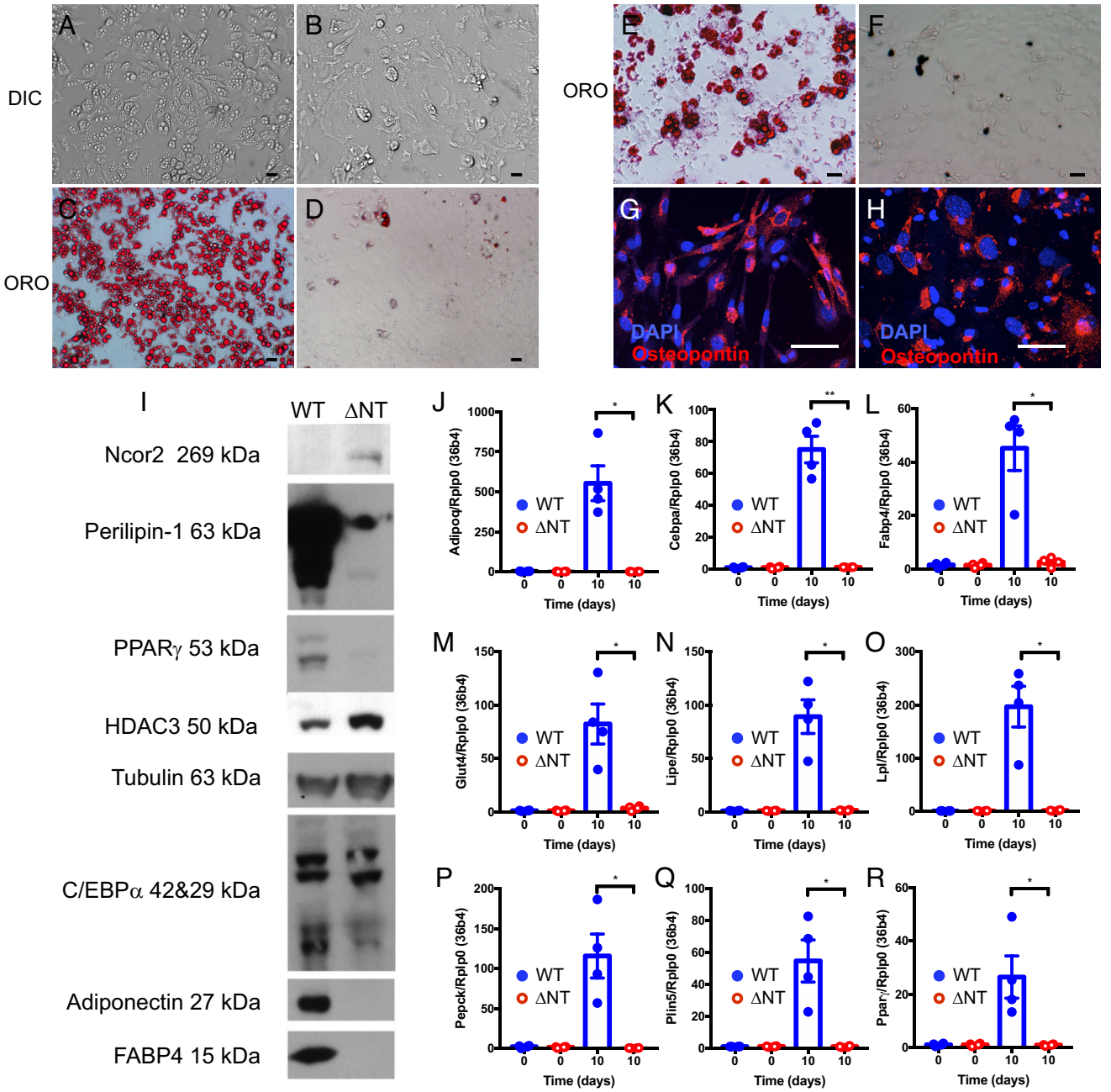

Fig. 5. Incomplete adipogenesis but normal osteoblastogenesis in ΔNT SVF and adipocytes. SVF cells were obtained after enzymatic digestion of SC WAT, and differentiated in adipogenic medium. More refringence, was observed in WT cells (*A*) than ΔNT cells (*B*) by phase contrast (DIC). Lipid droplets stained by Oil Red-O (ORO) in WT cells (*C*) are absent in ΔNT cells (*D*). ΔNT showed arrested adipogenesis. All scale bars, 20 μm. (*E* and *F*) MEF cells were differentiated in adipogenic medium and ORO-stained. Lipid droplets in WT (*E*), no lipid staining in ΔNT (*F*). (*G* and *H*) MEF were differentiated in osteogenic medium. Osteopontin stain (red) and DAPI counterstain (blue) were observed in osteoblasts after immunofluorescence by laser confocal microscopy. No differences in efficiency were seen between WT (*G*) and ΔNT (*H*). (*I*) Detection of adipogenesis markers in MEF by western blot. MEF were differentiated with the adipogenic cocktail and lysed. Several adipogenesis markers were detected (shown with expected molecular weights), including nuclear receptor corepressor 2 (Ncor2), perilipin-1, PPARγ, histone deacetylase 3 (HDAC3), α, alpha-tubulin 2 (tubulin), CAAT enhancer-binding protein C/EBPα, adiponectin, fatty acid binding protein 4 (FABP4). (*J*) *Adipoq*, (*K*) *Cebpa*, (*L*) *Fabp4*, (*M*) glucose transporter type 4 (*Glut4*), (*N*) hormone-sensitive lipase (*Lipe*), (*O*) *Lpl*, (*P*) phosphoenolpyruvate carboxykinase (*Pepck*), (*Q*) perilipin-5 (*Plin5*), and (*R*) *Pparγ* mRNA levels. For each gene, mRNA expression was calculated relative to *Rplp0* (*36b4*) expression. Gene expression analysis was performed in each genotype at steady state (0) set to one, and after 10-day differentiation (10); individual and mean ± SEM. WT: n = 4; ΔNT: n = 4.

model. Hypothermia is reversed by HFD, which suggests that the AT storage is inadequate to maintain core temperature. In rodents, decreased energy expenditure (EE) and hypothermia are linked to leptin deficiency and are restored by leptin therapy replacement. Low leptin levels with ectopic lipid accumulation, dyslipidemia, and insulin-resistant diabetes characterize lipodystrophic syndromes (8). Several lipodystrophic mouse models have been described with the absence of fat redistribution in liver, skeletal muscle, and pancreas (24, 34, 35). The ΔNT mice resemble these models, as they exhibit no glucose intolerance, hyperphagia, or metabolic impairments despite the relative absence of WAT. The ΔNT mice have controlled lipidemia with low body weight, even when fed with HFD.

Genetic causes of lipodystrophy are associated with BSCL2, AGPAT2, PPAR, PLIN1, CIDEC, or LIPE. We thus studied transcriptional responses to diet changes (CD and HFD) by comparing Epi WAT or SC WAT from WT and ΔNT mice. We studied transcriptional responses to diet changes (CD or HFD) by comparing Epi WAT from WT and ΔNT mice. The results showed

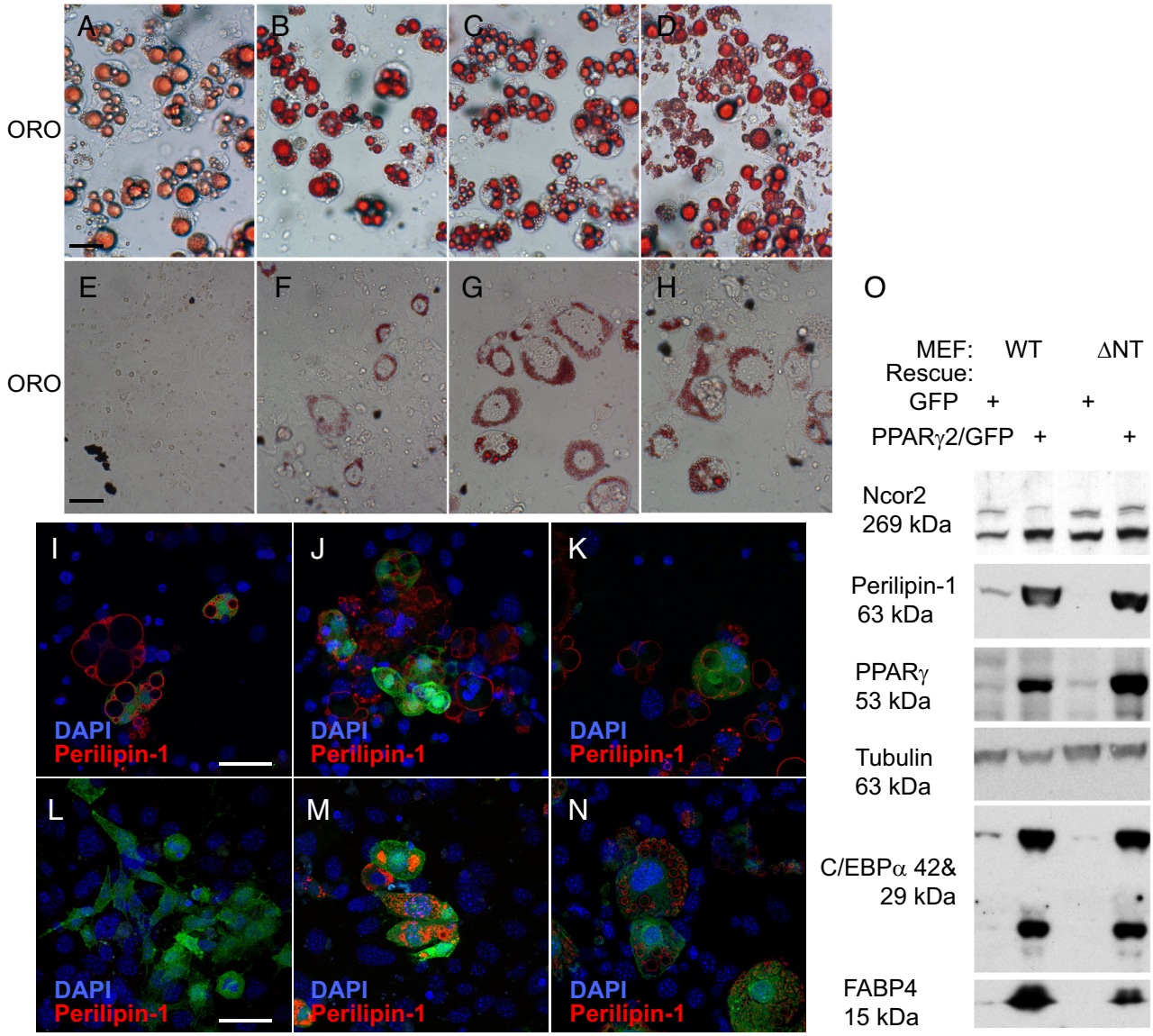

Fig. 6. Adipogenesis restoration in MEF from ΔNT mice by transcription factors Cebpa and Pparγ2. MEF from WT mice were infected with retroviral constructs for GFP as control (*A*) or with Cebpa/GFP (*B*), Pparγ2/GFP (*C*) or Cebpa/GFP + Pparγ2/GFP (*D*) and ΔNT MEF with retroviral constructs for GFP as control (*E*) or with Cebpa/GFP (*F*), Pparγ2/GFP (*G*) or Cebpa/GFP + Pparγ2/GFP (*H*). MEF were differentiated in adipogenic medium and neutral lipids were stained by ORO. MEF from ΔNT mice showed no lipid staining in control (*E*) but lipid droplets were restored by transcription factors. All scale bars, 20 μm. (*I-N*) Perilipin coats lipid droplets in differentiated MEF. WT MEF were infected with GFP as a control (*I*), Cebpa/GFP (*J*), or Pparγ2/GFP (*K*) and ΔNT MEF with GFP as a control (*L*), Cebpa/GFP (*M*), or Pparγ2/GFP (*N*). After adipogenic differentiation, immunofluorescence was detected by confocal microscopy after staining with anti-perilipin1 antibody (Perilipin, red) or DAPI (blue). Green light derives from the IRES-GFP-encoding viral vector used (see *Methods*). (*M* and *N*) Perilipin-coated lipid droplets are restored in ΔNT MEF. (*O*) Detection of adipogenesis markers in MEF by WB. GFP (GFP) or Pparγ2/GFP-transduced MEF were differentiated and lysed. Ncor2, perilipin-1, Pparγ, tubulin, C/EBPα, and FABP4 were detected in ΔNT MEF.

that CD led to the differential expression of 47 genes. This enabled us to establish a simplified list of markers that typifies our mouse model, including *Bscl2*, *Bcl6*, and *Rb4p*. *Bscl2* is linked to congenital lipodystrophy and is implicated in the formation of lipid droplets at an earlier stage than perilipins. In patients, *Bscl2* mutations lead to severe fat loss and other metabolic dysfunctions associated with lipodystrophy. Metabolic phenotypes are recapitulated in mice after general *Bscl2* KO, but unanticipated data were obtained following adipose tissue-specific deletion of *Bscl2*. Lipoatrophy was detected, but with limited hepatosteatosis, and no glucose intolerance or insulin resistance (35, 36). The lack of *Bscl2* classifies the ΔNT mice as lipodystrophic. Metabolic adaptation is observed in these mice with reduced AT. The gene *Bcl6* is a transcription repressor used as a marker to diagnose immune B cell lymphomas; it redistributes body fat following adipose tissue-specific deletion. *Bcl6* KO increases the SC WAT mass during development and enhances whole-body insulin sensitivity (25). Another marker, *Rpb4*, is an adipokine that triggers lipolysis and is engaged in the endocrine function of the liver and AT. High *Rbp4* levels are linked to T2D, metabolic syndrome, and obesity. Reduction of *Rbp4* in AT is monitored when weight loss is achieved by dietary intervention (26). The ADGAT KO mouse, which lacks two lipogenic enzymes, is another model of lipodystrophy with no ectopic fat accumulation in the liver, and resembles our ΔNT mice (35).

In HFD Epi WAT, functional analysis of transcriptomics experiments show increased gene expression for several categories. HFD is described to upregulate extracellular matrix (ECM) components and ECM remodeling genes (27, 37). Lipoatrophy can also originate from inaccurate differentiation or enhanced lipolysis activity. Subsequent to the hypolipidemia observed in our model, we

established a lipase or lipid biosynthesis signature associated with the RNAseq results; this list includes *Lipg*, *Pla2g16*, *Lipa*, *Pla1a*, *Pla2g7, and Pld3*. Phospholipases A2 and the lipase *Daglb* (diacylglycerol lipase-beta) release bioactive lipids that act on the endocannabinoid (EC) system, which ultimately controls fat storage and mobilization in AT (38). Other lipid metabolism genes, *Alox12* and *Faah*, were high, whereas the peripheral cannabinoid receptor *Cnr2* was low; all these genes form part of the EC pathway (see online tool: LIPIDMAPS, The Lipid Web, Lipidomics Gateway). This confirmed broad perturbation of EC signaling by diet (39) in the Epi WAT after HFD. There is an inverse relationship between endothelial lipase (*Lipg*) and HDL levels in mice (40). Our results showed more circulating HDL and less *Lipg* gene expression in WT mice. *Lipa,* lysosomal acid lipase (LAL), is increased in mice fed HFD (41), which coincides with our results in WT mice. Targeting the lipase pathway with the inhibitor orlistat is currently a successful pharmacological treatment for obesity.

Although *Plin1* is not a lipase gene, it greatly affects lipolysis. *Plin2*-null mice show fat mass reduction after HFD (42). The *Plin2* gene was up-regulated in our WT mice when fed with HFD. In vitro studies of perilipin require precise timing, as during adipogenesis PLIN2 coats early lipid droplets first and is later replaced by PLIN1. *Plin2* compensation for *Plin1* is another possibility. We found decreased PLIN1 in ΔNT MEF. Its upregulation following PPARγ rescue confirmed PLIN1 as a PPARγ target gene. Mutations in the PLIN1 gene are related to lipodystrophy.

Transferring microbiota from lean or obese patients triggers equivalent pathologies in mice (43). We cannot rule out microbiota differences that could influence our mouse model, and microbiota transfer experiments between the ΔNT and WT obese mice are options for the future.

Although other mouse models of lipodystrophy have been described, many directly involve lipid processing or storage pathways. A few models involve transcription factors such as PPARγ, which control key genes in adipocyte differentiation. Our prior studies showed that DIDO has no DNA-binding domain to target gene promoters but instead is enriched in actively transcribed genes through a histone-binding domain (13). DIDO forms a scaffold on the RNA POLII to recruit SFPQ and aid splicing of target transcripts (16). Removal of the N-terminal part of DIDO3 reduces enrichment in actively transcribed genes, partially suppressing the supportive role in RNA processing of binding proteins to the rest of the truncated protein structure. Here, we uncovered evidence that *Dido1* affects obesity through transcriptional programs that drive C/EBP- and PPAR-mediated adipogenesis. Ectopic expression of C/EBPα or PPARγ2 in fibroblasts commits the cells to mature as post-mitotic adipocytes, with a complete repertoire of adipose gene expression (29, 44). Adipogenesis-deficient ΔNT MEF were rescued by expressing C/EBPα, PPARγ2, or both in combination; this suggests that the ΔNT mouse fibroblasts are in a commitment stage that is permissive to both transcription factors. Given its role in transcription, we cannot exclude the possibility that C/EBP and PPARγ are target genes of *Dido1*.

Our results connect the N-terminal part of DIDO with adipogenesis and WAT development. An alternative is that, by preventing binding of partners to the DIDO N terminus, we could modify WAT development. We propose the DIDO PHD domain as an alternative target in screening strategies for small molecules that affect obesity and the metabolic syndrome.

Materials and Methods

Animals and Tissue Collection. Mixed genetic background ΔNT mice were generated as described (19) and backcrossed more than 10 times on a C57BL/6 background. Mice were maintained at 22 °C on a normal diet (ND; SAFE150) composed of 12.6% fat, on a 12/12-h light/dark cycle with ad libitum access to food and water (see *SI Appendix* for details). A control diet (CD)/high fat diet (HFD) pair was used to induce obesity, as recommended by the manufacturer [CD (Ssniff E15748) composed of 4.1% fat/HFD (Ssniff E15744) 45% fat].

After a 4-h fast, serum TG, LDL, HDL, and total cholesterol were measured in an automated analyzer (Siemens). Body temperatures were recorded by handheld digital rectal thermometer (AZ Instruments). Serum insulin was measured in a Luminex assay (EMD Millipore). Mice were handled according to national and European Union guidelines, and experiments were approved by the Comité Ético de Experimentación Animal, Centro Nacional de Biotecnología, Consejo Superior de Investigaciones Científicas.

AT Histology. AT were fixed before paraffin embedding and section. AT were hematoxylin–eosin (HE)-stained, and images of representative fields taken using a Nikon microscope (see *SI Appendix* for details).

SVF Isolation, Adipogenic Differentiation, and Oil Red Staining. See *SI Appendix* for details. SC WAT fat pads were excised, minced, and digested with proteases (Roche). Cells were filtered and centrifuged (700 g, 10 min). The infranatant (SVF) was washed and resuspended in complete DMEM/F-12. SVF cells were plated in collagen-coated plates and differentiated (2 d) with induction medium (FBS, IBMX, indomethacin, dexamethasone, insulin, T3, and rosiglitazone), followed by maintenance medium (FBS, insulin, T3, and rosiglitazone) for 7 d. Adipocytes were fixed and stained with an Oil Red-O solution (ORO; Sigma-Aldrich) and observed under the microscope.

Adipogenic and Osteogenic MEF Differentiation. Primary MEF cells were isolated and differentiated into adipocytes and ORO-labeled as above. Primary MEF were obtained from embryos and differentiated into osteoblasts using the mouse mesenchymal stem cell functional identification kit (R&D). After 20-d differentiation, osteoblasts were formalin-fixed, stained with an anti-osteopontin antibody, and counterstained with DAPI for observation by confocal microscopy.

Western Blot. Adipocytes were lysed in Triton lysis buffer [20 mM Tris (pH 7.4), 1% Triton X-100, 10% glycerol, 137 mM NaCl, 2 mM ethylenediaminetetraacetic acid, 25 mM β-glycerophosphate, 1 mM sodium orthovanadate, 1 mM phenylmethylsulfonyl fluoride, and 10 μg/mL aprotinin plus leupeptin]. Extracts (15 μg) were examined by protein immunoblot analysis by probing with antibodies to Ncor2, tubulin, PPAR-gamma, perilipin-1, HDAC3, C/EBPα, fatty acid-binding protein 4 (FABP4), and adiponectin (see *SI Appendix* for details), secondary horseradish peroxidase-conjugated antibodies (Dako), and an enhanced chemiluminescent luminol reagent kit (Santa Cruz).

RNA Isolation and Gene Expression Analysis by RT-PCR. RNA was extracted from tissues using Trizol (Thermo Fisher Scientific). RT-quantitative PCR (RT-qPCR) was conducted in technical triplicates using Fast SYBR Green assays (Thermo Fisher Scientific) on an ABI PRISM 7900HT thermocycler (Applied Biosystems). Relative mRNA expression was normalized to the housekeeping gene (HKG) *Rplp0* (*36b4*). See *SI Appendix* for details and primer list.

Gene Therapy. Concentrated viral particles encoding GFP alone, Cebpa/GFP, PPARγ2/GFP, or Cebpa/GFP + PPARγ2/GFP (see *SI Appendix* for cloning and packaging details) were used to infect WT or ΔNT MEF cells [MOI (multiplicity of infection) = 0.3] for 24 h. Four days after infection, transduced cells were differentiated to adipocytes as described above (IBMX, T3, DEXA, insulin, indomethacin, and rosiglitazone).

RNA-Sequencing and Functional Enrichment Analysis. RNA-Seq was performed in biological triplicates in Epi WAT of mice fed CD for 8 wk, followed by 13 wk of CD or HFD. Total RNA was purified with the Split RNA Extraction Kit (Lexogen). Libraries were prepared by the Genomics Unit of the Scientific Park Madrid and sequenced using NovaSeq 6000 or NexSeq 2000 High Output Run Mode V4 (Illumina) as single-end 100-bp reads. Transcripts were mapped to a mouse reference genome (GRCm38/mm10 assembly) using BWA-MEM. Alignments were formatted to BAM and duplicates were removed with Picard tools. Relative expression of transcripts was quantified with StringTie, converted to transcripts per million (TPM) reads, and kept for later analysis when

TPM > 0 in all samples. The expression level of all genes was estimated by DESeq2. Genes with a Benjamini–Hochberg adjusted *P*-value < 0.05 and a cut-off of 0.6 in logFC were considered differentially expressed (DEG). Data were obtained, processed, and annotated using R. Functional enrichment analysis was performed using g:Profiler, and heatmaps were built using Pheatmap. RNA-Seq data are deposited in the Gene Expression Omnibus under accession code GSE236036. The Excel spreadsheet of the RNA-seq analysis related to Fig. 4 and *SI Appendix*, Figs. S8, S10, and S11 is found as supporting material in Dataset S1. The Excel spreadsheet of the functional enrichment analysis related to Fig. 4 and *SI Appendix*, Figs. S9 and S10 is found in Dataset S2.

Statistics. Data are individual and mean ± SEM. Statistical analysis was performed in GraphPad Prism. Comparisons between two groups were performed with unpaired two-tailed Student's *t* test and multiple group comparisons by ANOVA. $P \leq 0.05$ was considered statistically significant. not significant (NS), $*P < 0.05$; $**P < 0.01$; $***P < 0.001$; $****P < 0.0001$ vs. controls.

Data, Materials, and Software Availability. RNA sequencing data have been deposited in Gene Expression Omnibus (GSE236036) (45).

ACKNOWLEDGMENTS. We thank Ana Paredes of the Spanish National Cardiovascular Research Center (CNIC), Madrid for the gift of pHR SIN viral vector and advice on RNA-Seq. We also thank Luis Almonacid from the CNB Genomics Unit RT-qPCR facility, and Catherine Mark for editorial assistance. This work was supported by grants PID2019-110574RB-I00 and PID2022-142616OB-100 from the Spanish Ministerio de Ciencia e Innovacion, grant P2022/BMD-7321 (MITIC-CM) from the Comunidad de Madrid, and a grant from the BBVA Foundation ("The role of Dido").

Author affiliations: [a]Department of Immunology and Oncology, Centro Nacional de Biotecnología-Consejo Superior de Investigaciones Científicas Campus, Universidad Autónoma de Madrid, Madrid 28049, Spain; [b]Centro Nacional de Investigaciones Cardiovasculares, Madrid 28029, Spain; and [c]Department of Basic Sciences of Health, Area of Biochemistry and Molecular Biology, Universidad Rey Juan Carlos, Alcorcon 28922, Spain

1. D. Albuquerque, C. Nóbrega, L. Manco, C. Padez, The contribution of genetics and environment to obesity. *Br. Med. Bull.* **123**, 159–173 (2017).
2. E. D. Rosen, B. M. Spiegelman, Adipocytes as regulators of energy balance and glucose homeostasis. *Nature* **444**, 847–853 (2006).
3. G. S. Hotamisligil, N. S. Shargill, B. M. Spiegelman, Adipose expression of tumor necrosis factor-alpha: Direct role in obesity-linked insulin resistance. *Science* **259**, 87–91 (1993).
4. NCD Risk Factor Collaboration, Trends in adult body-mass index in 200 countries from 1975 to 2014: A pooled analysis of 1698 population-based measurement studies with 19·2 million participants. *The Lancet* **387**, 1377–1396 (2016).
5. B. Knebel, D. Müller-Wieland, J. Kotzka, Lipodystrophies–disorders of the fatty tissue. *Int. J. Mol. Sci.* **21**, 8778 (2020).
6. A. Guilherme, J. V. Virbasius, V. Puri, M. P. Czech, Adipocyte dysfunctions linking obesity to insulin resistance and type 2 diabetes. *Nat. Rev. Mol. Cell Biol.* **9**, 367–377 (2008).
7. M. Petruzzelli *et al.*, A switch from white to brown fat increases energy expenditure in cancer-associated cachexia. *Cell Metab.* **20**, 433–447 (2014).
8. I. W. Asterholm, N. Halberg, P. E. Scherer, Mouse Models of Lipodystrophy Key reagents for the understanding of the metabolic syndrome. *Drug Discov. Today Dis. Models* **4**, 17–24 (2007).
9. S. Le Lay, J. Magré, X. Prieur, Not enough fat: Mouse models of inherited lipodystrophy. *Front. Endocrinol.* **13**, (2022).
10. D. B. Savage, Mouse models of inherited lipodystrophy. *Dis. Model. Mech.* **2**, 554–562 (2009).
11. V. Trachana, K. H. M. van Wely, A. A. Guerrero, A. Fütterer, C. Martínez-A, Dido disruption leads to centrosome amplification and mitotic checkpoint defects compromising chromosome stability. *Proc. Natl. Acad. Sci. U.S.A.* **104**, 2691–2696 (2007).
12. A. Fütterer *et al.*, Ablation of Dido3 compromises lineage commitment of stem cells in vitro and during early embryonic development. *Cell Death Differ.* **19**, 132–143 (2012).
13. J. Gatchalian *et al.*, Dido3 PHD modulates cell differentiation and division. *Cell Rep.* **4**, 148–158 (2013).
14. A. Fütterer *et al.*, DIDO as a switchboard that regulates self-renewal and differentiation in embryonic stem cells. *Stem Cell Rep.* **8**, 1062–1075 (2017).
15. A. M. Rojas *et al.*, Death inducer obliterator protein 1 in the context of DNA regulation. Sequence analyses of distant homologues point to a novel functional role. *FEBS J.* **272**, 3505–3511 (2005).
16. C. Mora Gallardo *et al.*, Dido3-dependent SFPQ recruitment maintains efficiency in mammalian alternative splicing. *Nucleic Acids Res.* **47**, 5381–5394 (2019).
17. A. Fütterer *et al.*, Impaired stem cell differentiation and somatic cell reprogramming in DIDO3 mutants with altered RNA processing and increased R-loop levels. *Cell Death Dis.* **12**, 637 (2021).
18. K. Jain *et al.*, Characterization of the plant homeodomain (PHD) reader family for their histone tail interactions. *Epigenet. Chromatin* **13**, 3 (2020).
19. A. Fütterer *et al.*, Dido gene expression alterations are implicated in the induction of hematological myeloid neoplasms. *J. Clin. Invest.* **115**, 2351–2362 (2005).
20. S. C. Benoit, D. J. Clegg, R. J. Seeley, S. C. Woods, Insulin and leptin as adiposity signals. *Recent Prog. Horm. Res.* **59**, 267–285 (2004).
21. G. Maor, M. Rochwerger, Y. Segev, M. Phillip, Leptin acts as a growth factor on the chondrocytes of skeletal growth centers. *J. Bone Miner. Res.* **17**, 1034–1043 (2002).
22. H. Wang *et al.*, Adipose tissue transplantation ameliorates lipodystrophy-associated metabolic disorders in seipin-deficient mice. *Am. J. Physiol.-Endocrinol. Metab.* **316**, E54–E62 (2018).
23. S. Zhao *et al.*, Partial leptin reduction as an insulin sensitization and weight loss strategy. *Cell Metab.* **30**, 706–719.e6 (2019).
24. L. Dollet *et al.*, Seipin deficiency alters brown adipose tissue thermogenesis and insulin sensitivity in a non-cell autonomous mode. *Sci. Rep.* **6**, 35487 (2016).
25. M. D. Senagolage *et al.*, Loss of transcriptional repression by BCL6 confers insulin sensitivity in the setting of obesity. *Cell Rep.* **25**, 3283–3298.e6 (2018).
26. J. S. Steinhoff, A. Lass, M. Schupp, Biological functions of RBP4 and its relevance for human diseases. *Front. Physiol.* **12**, (2021).
27. M.-J. Lee, Y. Wu, S. K. Fried, Adipose tissue remodeling in pathophysiology of obesity. *Curr. Opin. Clin. Nutr. Metab. Care* **13**, 371–376 (2010).
28. E. D. Rosen, O. A. MacDougald, Adipocyte differentiation from the inside out. *Nat. Rev. Mol. Cell Biol.* **7**, 885–896 (2006).
29. P. Tontonoz, E. Hu, B. M. Spiegelman, Stimulation of adipogenesis in fibroblasts by PPAR gamma 2, a lipid-activated transcription factor. *Cell* **79**, 1147–1156 (1994).
30. D. Merrick *et al.*, Identification of a mesenchymal progenitor cell hierarchy in adipose tissue. *Science* **364**, eaav2501 (2019).
31. J. Martinez-Botas *et al.*, Absence of perilipin results in leanness and reverses obesity in Leprdb/db mice. *Nat. Genet.* **26**, 474–479 (2000).
32. X.-D. Peng *et al.*, Dwarfism, impaired skin development, skeletal muscle atrophy, delayed bone development, and impeded adipogenesis in mice lacking Akt1 and Akt2. *Genes Dev.* **17**, 1352–1365 (2003).
33. E. D. Rosen *et al.*, C/EBPα induces adipogenesis through PPARγ: A unified pathway. *Genes Dev.* **16**, 22–26 (2002).
34. G. D. Mcilroy *et al.*, Adipose specific disruption of seipin causes early-onset generalised lipodystrophy and altered fuel utilisation without severe metabolic disease. *Mol. Metab.* **10**, 55–65 (2018).
35. C. Chandramohan *et al.*, Mice lacking triglyceride synthesis enzymes in adipose tissue are resistant to diet-induced obesity. *ELife* **12**, (2023).
36. G. D. Mcilroy, S. E. Mitchell, W. Han, M. Delibegović, J. J. Rochford, Ablation of Bscl2/seipin in hepatocytes does not cause metabolic dysfunction in congenital generalised lipodystrophy. *Dis. Model. Mech.* **13**, dmm042655 (2020).
37. F. J. Ruiz-Ojeda, A. Méndez-Gutiérrez, C. M. Aguilera, J. Plaza-Díaz, Extracellular matrix remodeling of adipose tissue in obesity and metabolic diseases. *Int. J. Mol. Sci.* **20**, 4888 (2019).
38. V. Di Marzo, I. Matias, Endocannabinoid control of food intake and energy balance. *Nat. Neurosci.* **8**, 585–589 (2005).
39. E. N. Kuipers *et al.*, High fat diet increases circulating endocannabinoids accompanied by increased synthesis enzymes in adipose tissue. *Front. Physiol.* **9**, 1913 (2019).
40. T. Ishida *et al.*, Endothelial lipase is a major determinant of HDL level. *J. Clin. Invest.* **111**, 347–355 (2003).
41. C. Gamblin *et al.*, Lysosomal acid lipase drives adipocyte cholesterol homeostasis and modulates lipid storage in obesity, independent of autophagy. *Diabetes* **70**, 76–90 (2021).
42. J. L. McManaman *et al.*, Perilipin-2-null mice are protected against diet-induced obesity, adipose inflammation, and fatty liver disease. *J. Lipid Res.* **54**, 1346–1359 (2013).
43. V. K. Ridaura *et al.*, Gut microbiota from twins discordant for obesity modulate metabolism in mice. *Science* **341**, 1241214 (2013).
44. S. O. Freytag, D. L. Paielli, J. D. Gilbert, Ectopic expression of the CCAAT/enhancer-binding protein alpha promotes the adipogenic program in a variety of mouse fibroblastic cells. *Genes Dev.* **8**, 1654–1663 (1994).
45. M. A. García-López, T. Pons, C. Martínez-A, T. Fischer, DIDO is necessary for the adipogenesis that promotes diet-induced obesity. NCBI GEO. https://www.ncbi.nlm.nih.gov/geo/query/acc.cgi?acc=GSE236036. Deposited 28 June 2023.